Nuclear Inst. and Methods in Physics Research, A 908 (2018) 236–243

Contents lists available at ScienceDirect

Nuclear Inst. and Methods in Physics Research, A

journal homepage: www.elsevier.com/locate/nima

Towards in-jet resonance ionization spectroscopy: An injection-locked Titanium:Sapphire laser system for the PALIS-facility

M. Reponen [a,b,*], V. Sonnenschein [c,b], T. Sonoda [b], H. Tomita [c,b], M. Oohashi [c], D. Matsui [c], M. Wada [b]

[a] Department of Physics, University of Jyväskylä, PO Box 35 (YFL), Jyväskylä FI-40014, Finland
[b] RIKEN Nishina Center for Accelerator-Based Science, 2-1 Hirosawa, Wako, Saitama 351-0198, Japan
[c] Department of Energy Engineering, Nagoya University, Nagoya 464-8603, Japan

ARTICLE INFO

Keywords:
Laser ion source
Laser development
Laser resonance ionization
Laser spectroscopy

ABSTRACT

This article presents a pulsed narrowband injection-locked Titanium:Sapphire laser aimed for high-resolution in-jet resonance ionization spectroscopy at the SLOWRI/PALIS at RIKEN. The laser has been integrated into the PALIS laser laboratory enabling it to be utilized with the existing broadband Titanium:Sapphire and dye lasers. The seed efficiency has been evaluated to be close to unity over the master laser wavelength range ~ 753 to 791 nm, and the slope efficiency, namely the ratio of the pump power to the output power, was determined to be ~ 30 % at 780 nm. A two-step ionization scheme with 386.4016 nm first step and 286.731 nm second step into an autoionizing state was developed for resonance ionization spectroscopy of ^{93}Nb. Magnetic hyperfine coupling constants of 1866 ± 8 MHz and 1536 ± 7 MHz were measured for the ground and excited state, respectively, in a good agreement with the literature values. A Gaussian dominated Voigt linewidth of 434.5 ± 7.4 MHz was extracted from the hyperfine spectra measured for niobium. In addition, the resolution of the in-jet resonance ionization in PALIS is estimated through numerical methods.

1. Introduction

Hyperfine structures and isotope shifts in electronic transitions contain readily available model-free information [1] on the single-particle and bulk properties of exotic nuclei, namely the nuclear spin, magnetic dipole and electric quadrupole moments as well as changes in root-mean-square charge radii [2]. The part-per-million level perturbations of the atomic energy levels of an atom caused by its nucleus are readily probed by modern laser spectroscopic methods. Resonance ionization spectroscopy (RIS) [3] is a selective and efficient method built upon the unique excitation energies of atomic states of different elements for a step-wise excitation and subsequent ionization of an atom.

Through recent innovations in gas cell technology and laser techniques, RIS in-source has been demonstrated to be a powerful tool for probing rare nuclei with lifetimes as short as a few milliseconds and production rates often only a few isotopes of interest per second [4,5]. Typically, the laser ion sources at RIB facilities have linewidths of few gigahertz to maximize the ionization efficiency by covering the entire the Doppler ensemble in-source, and only in selected cases is the hyperfine splitting large enough to be resolved.

Recently, the implementation of RIS in a low-temperature supersonic gas jet [6,7] utilizing a narrowband first step excitation has gained considerable interest [8]. An optimal solution to combine high pulse powers required for efficient ionization with a narrow linewidth is the pulsed amplification of a narrow-band continuous wave (CW) laser. While for high-gain dye lasers a single pass amplification is sufficient, the lower gain Titanium:Sapphire gain medium requires a different approach. In a regenerative amplifier, the cavity length is locked to a multiple of the seed wavelength allowing Titanium:Sapphire-based lasers to reach a final output power of several kW (during the pulse) from the few mW of CW input.

A previous iteration of the laser presented in this article, was designed and tested offline at the University of Jyväskylä [9,10] on stable Cu isotopes, and later applied to high-resolution RIS of Ac, Pu and Th [11,9,12,13] at University of Mainz. Furthermore, the previous iteration has been successfully applied to online studies of ^{214,215}Ac in the vicinity of the $N = 126$ neutron shell closure in LISOL-facility in Belgium [14] and of $^{73-78}$Cu in CRIS [15] experiment in CERN-ISOLDE [16]. In this work, we present a pulsed injection-locked Titanium:Sapphire laser operating at 10 kHz repetition rate aimed for future in-jet spectroscopy at the SLOWRI/PALIS at RIKEN, apply it for RIS of Nb in vacuum and numerically estimate the resolution of in-jet RIS in counter-propagating geometry.

* Corresponding author at: Department of Physics, University of Jyväskylä, PO Box 35 (YFL), Jyväskylä FI-40014, Finland.
E-mail address: mikael.h.t.reponen@jyu.fi (M. Reponen).

https://doi.org/10.1016/j.nima.2018.08.073
Received 17 April 2018; Received in revised form 27 July 2018; Accepted 22 August 2018
Available online xxxx

2. Experimental setup

The slow RI-beam facility (SLOWRI) [17] at the RI Beam Factory (RIBF) [18] accelerator complex of the RIKEN Nishina Center for Accelerator-Based Science is being developed towards precision mass [19] and atomic spectroscopy [20] of rare isotopes. Using RF-carpet ion guides, the facility will provide a broad selection of low-energy isotopic beams of all elements produced through projectile fragmentation and in-flight fission reactions in the BigRIPS. However, the use of the SLOWRI gas stopper requires primary machine time at the BigRIPS ; hence the available time for experiments will be restricted by the limited operation time. To address this issue a new gas stopper, namely PALIS—PArasitic RI-beam production by Laser Ion Source, was proposed [21,22].

With the PALIS approach, the 200 MeV/u in-flight reaction products are stopped in 25 cm long gas cell located the second focal plane chamber the BigRIPS separator. The stopped products are promptly neutralized by high purity atmospheric pressure argon buffer gas, transported towards an ⌀ 1 to 2 mm exit hole by the gas flow in 1–300 ms and subsequently selectively re-ionized using 10 kHz repetition rate pulsed lasers. Due to large atom density, the ionization mainly takes around the exit hole region both in gas cell and in a supersonic gas-jet within a SextuPole Ion-beam Guide (SPIG) [23]. The ions are assisted through the SPIG by the gas flow and into a quadrupole mass separator after which they detected by a channeltron detector located in a high-vacuum region. The extreme pressure difference from atmospheric conditions to 10^{-3} Pa is achieved by using a novel differential pumping setup described in Ref. [24].

The novel idea behind the PALIS catcher is that it extends the available beam time at SLOWRI due its ability to run parasitically along primary experiments and utilize the otherwise discarded reaction products. Besides being a production device, PALIS has also been designed for in-jet RIS. The following sections describe a pulsed injection-locked Titanium:Sapphire laser system based on design presented in Ref's [25,26,10], aimed for high-resolution in-jet RIS. Furthermore, the laser is commissioned through RIS of ^{93}Nb in vacuum.

Niobium was chosen as the test case due to experimental considerations, e.g. convenient transition frequencies considering the injection-locked Titanium:Sapphire, and for the possibility to apply the laser developments to future research projects. As niobium has only a single stable isotope, no mass separation is required and the experimental setup can be simplified considerably. In addition, the atomic structure for niobium is well documented (see Ref's [27–30]), thus enabling convenient evaluation of the accuracy of the setup.

Only limited optical spectroscopy has been performed on radioactive niobium isotopes [31] due to the refractory nature of the element which makes it difficult to produce with the standard thick target ISOL (Isotope Separation On-Line) method. However, high-resolution RIS capability at a gas-cell-based production facility such as PALIS would open a possibility for future on-line studies along the niobium isotopic chain. In addition, the isomer ^{93m}Nb($T_{1/2}$ = 16.13 a) has been proposed to be utilized in an integrated fast neutron dosimetry of nuclear reactor vessel and structures via resonance ionization mass spectrometry (RIMS) [28]. This technique aims to separate the ground state from the isomer ^{93m}Nb, and it requires a narrowband laser to drive a transition with a large enough hyperfine splitting that can efficiently provide sufficient spectral selectivity [32]. Previous work utilizing Titanium:Sapphire lasers for this purpose can be found in Ref's [33,34].

2.1. PALIS laser system

The injection-locked Titanium:Sapphire laser has been designed to operate as a part of the PALIS-laser laboratory, described in detail in Ref. [23]. Two distinct laser systems (see Fig. 1 for a schematic layout) were utilized in this experiment. The first system is formed by two Sirah/Credo dye lasers pumped by a 10 kHz Edgewave Nd:YAG

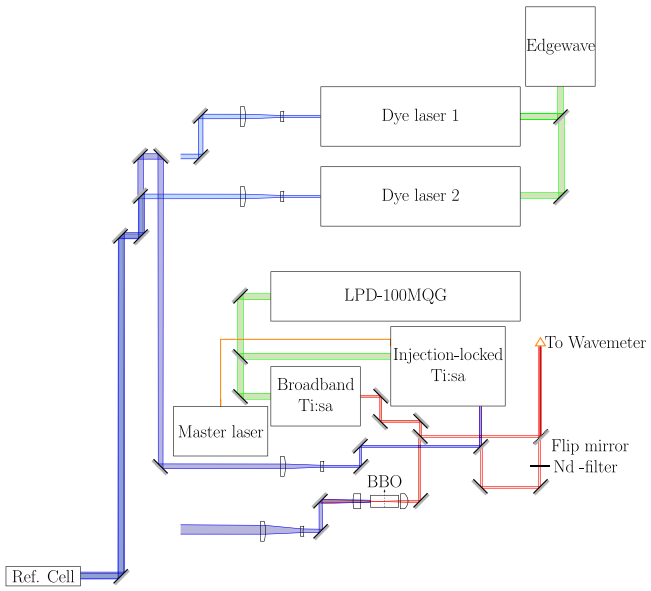

Fig. 1. A schematic optical table configuration at PALIS. The figure shows an overlap between the injection-locked Titanium:Sapphire and Dye laser 2 beams, but the systems allowed also dye laser 1 and the broadband Titanium:Sapphire to be utilized with the injection-locked Titanium:Sapphire.

InnOSlab. The pump power can be split between the dye laser in various ways to produce up to 10 W average fundamental output power, which further converts to ~1 W on the second harmonic with the linewidth in the GHz-region and a pulse width of ~10 ns.

The second laser system is a Titanium:Sapphire-based laser set-up pumped by a 10 kHz Nd:YAG (Lee Laser LDP-100MQG). The system consists of two lasers with one being a commercial broadband Titanium:Sapphire laser (Radiant Dyes) and the other laser is the in-house designed injection-locked Titanium:Sapphire laser. The broadband laser has a Z-shape cavity with an Etalon and a Birefringent filter resulting in a typical fundamental linewidth of 3–5 GHz, and an output power of ≤4 W with ~35 ns pulse width.

Additionally the Titanium:Sapphire laser setup includes a single-pass harmonic generation setup capable of efficient generation of 2nd, 3rd and 4th harmonics. The setup also includes a precise beam shaping system realized with cylindrical lenses and beam expanders used compensate for beam astigmatism and divergence resulting from the harmonic generation, and to prepare the beam for the long transport to PALIS.

The pump lasers share a common master trigger, from which the signal is divided between the two pump lasers. The trigger for the Edgewave is passed through an Ortec 416A gate and delay generator to allow temporal synchronization of the output pulses from the dye lasers and the Titanium:Sapphire lasers. The two Titanium:Sapphire laser can further be synchronized by detuning either the laser cavities or the pump beam alignment.

When utilized for resonance ionization at the PALIS, the laser beams are expanded by a ~ factor of 10, combined on the optical table and transported with more than 50% efficiency over a 70 m long optical path to the PALIS gas cell realized with broadband mirrors on a motorized mirror mounts [23].

2.2. Injection-locked Titanium: Sapphire laser

The lasers introduced in the preceding section were designed to operate in the GHz linewidth region to efficiently drive transitions in a high-pressure gas-cell environment. The injection-locked Titanium:Sapphire laser presented in this section, however, aims for resonance ionization

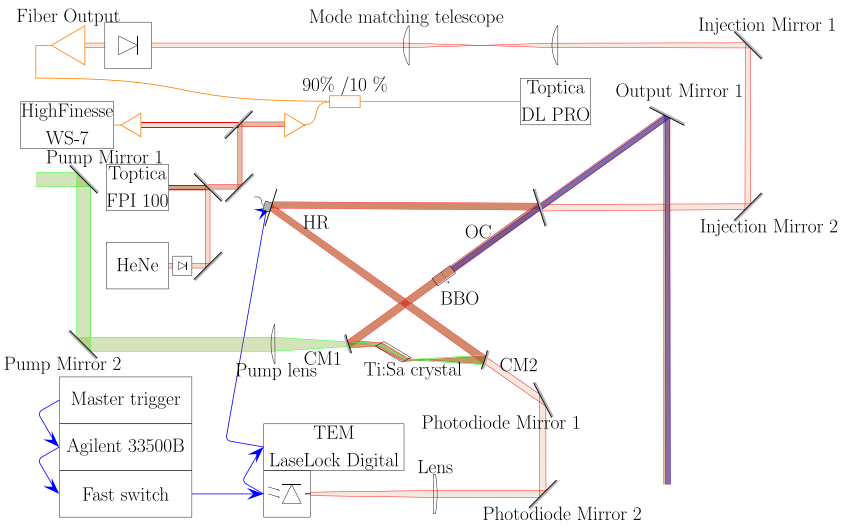

Fig. 2. A schematic view of the injection-locked Titanium:Sapphire-setup.

spectroscopy in a supersonic gas-jet, where Doppler and pressure broadening mechanisms are greatly reduced.

The operation of a injection-locked Titanium:Sapphire set-up presented in Fig. 2 requires two different laser system, namely a Master and a Slave laser. The preferable requirements for a master laser include CW operation, a broad tuning range and a narrow linewidth. While these characteristics are readily found in a CW Titanium:Sapphire lasers, in this work an extended cavity diode laser (ECDL), Toptica DL Pro equipped with a 780 nm diode, was used. The laser provides a sub MHz linewidth with more than 20 GHz mode-hop free tuning range and high peak output power in the 780 nm wavelength region. A wide mode-hop free tuning range is necessary for the spectroscopy of elements with large hyperfine splitting, for example ~20 MHz in the case of ^{93}Nb. A Master laser mode-hop would cause the Slave laser to lose lock and hence cause the laser to lase in free-running, broadband mode. While to lock may recover after the mode-hop, the jump in the laser frequency is usually large enough to severely disturb any ongoing measurement.

A 10% fraction Master laser output was divided between a HighFinesse WS7 wavemeter and a Toptica FPI 100 Fabry–Pérot interferometer (FSR 1 GHZ), the latter could be used to monitor the mode structure of the diode laser and detect possible multimode operation. The rest of the Master laser output was fiber coupled into the Slave laser through an integrated fiber coupler and internal optical isolator using a single-mode fiber.

The advancements over the previous iterations [10] were aimed to improve stability, usability and vibration sensitivity. Optimal locations for the baseplate feet were numerically determined through FEM simulations, and the cavity mirrors (Thorlabs GM100/M) were mounted directly on a 30 mm thick aluminum baseplate in order to minimize the overall beam height. The FEM simulations additionally showed that the overall stability against vibrations was improved by a nearly a factor 50 over the previous design. In order to ease reproducibility and to further reduce external influence on the laser operation, the position of the cavity mirror mounts are determined by Dowell pins and the baseplate was designed to contain most of the required optical components. The components housed on the baseplate include the fiber input, mode matching optic for the master laser beam, fast optical diode system and output optics. This allows, for example, Master laser setup modifications without affecting the alignment of the injection beam in to Slave cavity.

The laser cavity is arranged in a bowtie geometry as seen in Fig. 2. The geometry, calculated by utilizing ray transfer matrices [35], was adapted from the previous iterations presented in [9,25]. The laser gain medium is a 20 mm long Brewster cut Titanium:Sapphire crystal (Absorption coefficient of $\alpha_{532} = 1.5\ \mathrm{cm}^{-1}$) mounted between two curved mirrors (CM1 and CM2, R = 75 mm) at a folding angle of 17.75°. In this setup, up to 25 W of pump power can be focused into the crystal through the CM1 mirror with an f = 75 mm pump lens. To dissipate the excess heat, the crystal is covered with a thin indium foil and clamped in a water-cooled copper mount. The baseplate design allows the crystal to be placed either symmetrically or asymmetrically between the curved mirrors. The symmetric crystal position enables higher gain and lower lasing threshold while sacrificing the output power due to worse mode matching with the pump beam compared to the asymmetric position [9].

The two other mirrors required to complete the cavity are the output coupler (OC), and the high reflector (HR) mounted on a Piezo actuator (Piezomechanik, PSt 150/10/20 VS15). The Piezo-actuated mirror was used to stabilize the laser via cavity length modulations using so-called dither locking technique with phase sensitive detection. An input signal for the locking electronics (TEM Messtechnik, LaseLock 3.0 Digital) was measured using a fast switching photodiode from the leakage through the CM2 mirror. A gate signal from a Master trigger driven waveform generator (Agilent 33500B) was fed into the photodiode to ground the electronics during a laser pulse from the Slave laser and thus to prevent the diode from saturating for extended periods. The locking electronics then dithered the signal using the Piezo-mounted HR-mirror to generate the error signal required by the PID regulator feedback loop.

In addition, the baseplate allows Piezo-mounted mirror and the high reflector mirror to be located in two different positions, to form a cavity with round-trip lengths either 580 mm or 420 mm. The longer cavity round-trip configuration allows the tuning range to be extended using birefringent filter [10] and the utilization of intra-cavity second harmonic generation [36], while the shorter can be used to produce shorter pulses. For a more detailed description of an injection-locked Titanium:Sapphire laser and the associated locking electronics see Ref. [10].

3. Laser characteristics

The target specifications for the laser include a linewidth of 20 MHz and a tuning range covering the majority of the Titanium:Sapphire gain band, coupled with high average output power and stability [10]. In this section, we present the tuning range and the seed efficiency for the particular set-up.

The tuning range of an injection-locked laser is limited by the Titanium:Sapphire gain band (~660–1000 nm), and dependent on the Master laser tuning range and on the optics used in the Slave laser cavity. When using a diode laser, a selection of diodes are available to cover the entire Titanium:Sapphire gain band. However, a continuous-wave Titanium:Sapphire laser would be a more convenient Master laser option

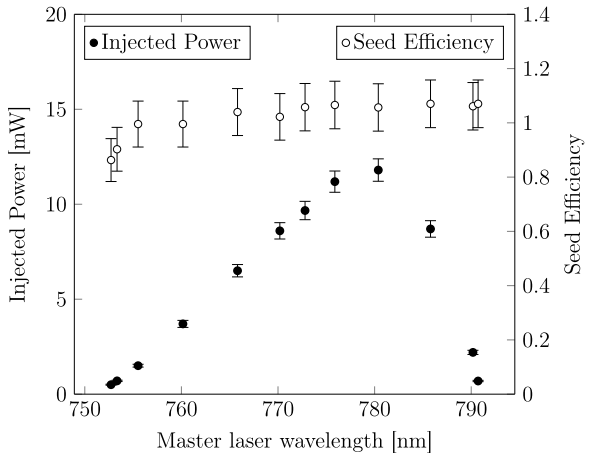

Fig. 3. Seed efficiency and the seed laser power as a function of the Master laser wavelength. The injected laser power is directly proportional to the Master laser output power.

as it provides a gapless wavelength range with generally much higher power and wider mode-hop free tuning range.

Furthermore, while the output power from the Master laser may be high the optical components along the injection path such as the optical isolator, induce losses so that only a part of the initial power is available for injection into the cavity. Especially, when using broadband cavity optics and going towards the limits of the Titanium:Sapphire gain band, the mode competition from the high-gain modes requires high injected power to force the laser to follow the Master laser wavelength. To get past these limitations, either dedicated optics sets or birefringent plates are required [10].

The intra-cavity second-harmonic option extends the direct laser output range to the visible and UV range which can be further used to generate wavelengths to the deep UV-region with high efficiency. As the seed laser needs to be injected, a constant fundamental light output is always present enabling a convenient sum-frequency mixing option to access wavelengths in the ~250–330 nm region.

In this work, the DL Pro master laser was equipped with a diode with a gain peak at 780 nm. The Slave laser cavity optics varied from narrowband curved mirrors (CM: Layertec 750–820 nm) to broadband output coupler (OC: Layertec 620–1020 nm 90%) and the high reflector Piezo-actuated mirror (HR: Thorlabs E03 750–1000 nm). Fig. 3 presents the seed efficiency (defined as the ratio of the locked output power and free running output power), and the injected power after the optical isolator as a function of the master laser wavelength. In this high-gain region even a small, sub mW injected power allows the Slave laser cavity to be locked with high seed efficiency. However, beyond the master laser wavelength range shown in Fig. 3, the Slave resonator operates only in free-running-mode where the narrow linewidth is lost essentially limiting the narrowband tuning range to ~750 – −790 nm.

When utilizing the intra-cavity second-harmonic generation option the effective outcoupling factor from the cavity is increased. In addition, the cavity losses are increased due to the additional crystal in the cavity, thus reducing the injected power circulating in the resonator. These factors can have an effect on the tuning range in addition to the properties of the non-linear crystal in use. However, when scanning the laser across a mode-hop free range there is no significant change in output power. With the intra-cavity setup, a second harmonic output power of 420 mW was achieved. The fundamental output power without the intra-cavity setup was ~4.2 W for the same pump power. In general, the output power at this setup was limited by the E03 mirror damage threshold.

The slope efficiency, extracted from a plot of pump power against the output power, is an important value in describing the laser performance.

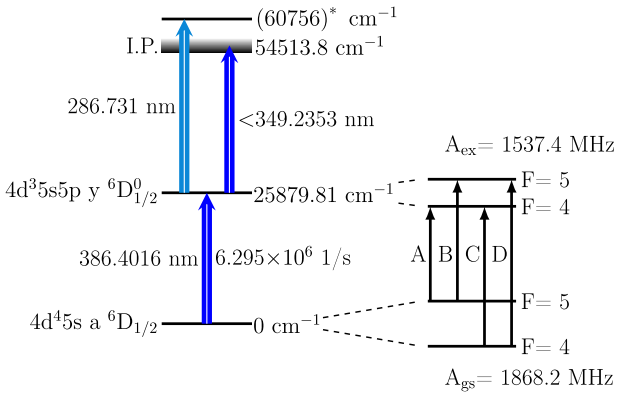

Fig. 4. Resonance ionization schemes for niobium utilized in this work, the individual hyperfine transitions are marked for clarity. The auto-ionizing state denoted with * was discovered in this work. The literature values for the magnetic hyperfine coupling constants (denoted as A_{gs} and A_{ex}) are from Ref. [27].

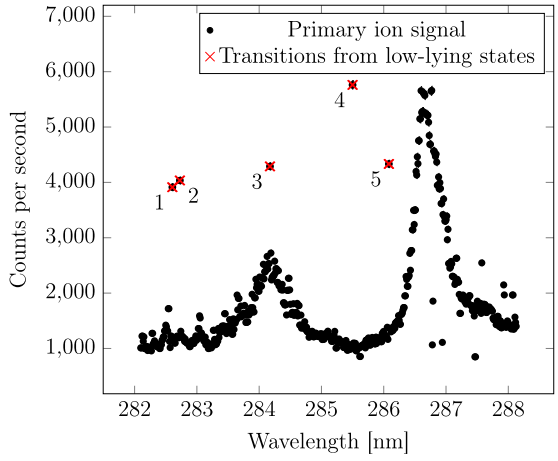

Fig. 5. A scan for autoionizing states using the dye laser. Additional single-color ionization channels are visible via a low-lying thermally populated states (see Table 1). (For interpretation of the references to color in this figure legend, the reader is referred to the web version of this article.)

For example insufficient crystal cooling leading to thermal lensing and reduced conversion efficiency at high pump powers would present itself as a deviation from linearity. A slope efficiency of $30 \pm 1\%$ extracted for the laser which is in agreement with the previous laser iteration.

4. Resonance ionization spectroscopy of niobium

The laser tuning range, when using the configuration described here, enables access to ground state transitions in multiple elements with great nuclear physics interest, for example, in the refractive element region where only a small number optical studies has been performed on radioactive isotopes [37]. As discussed earlier, niobium was chosen as the test case to demonstrate the laser application to high-resolution RIS.

The spectroscopy of niobium was performed in a reference cell where an atomic beam of niobium was generated by resistively heating a thin, 0.127–0.25 mm diameter, filament with 5–8 A DC current. The atomic beam was collimated with a narrow orifice, stepwise excited and subsequently ionized in a crossed beam geometry using the laser ionization schemes presented in Fig. 4. The ions were finally extracted into a channeltron detector.

The injection-locked Titanium:Sapphire laser was used to drive the first step transition in the ionization scheme at 386.4016 nm through the intra-cavity second harmonic generation of the fundamental wavelength

at around 782.8032 nm. The hyperfine splitting is 9.2 GHz for the ground state and 8.1 GHz for the first excited state [38] leading to very broad spectra compared to the laser linewidth. Therefore, the laser intensity at the ionization region was initially kept high to generate ion signal even in a case of a possible mismatch between the actual transition frequency and the calculated hyperfine transition (transition B in Fig. 4) at which the laser was set. Once a stable ion signal was achieved, the laser intensity was reduced by defocusing the first step laser to suppress power broadening and saturation effects.

A second step laser wavelength below ~349 nm was required to reach the ionization potential. This was readily achievable either with the broadband Titanium:Sapphire or the Dye lasers. Initially, the ionization scheme was realized with the Titanium:Sapphire laser system with external single pass second harmonic generation, where the ionizing transition to continuum just above the ionization potential was driven by the broadband laser (Fig. 1).

However, in RIS the ionizing transition plays a significant role in the efficiency of the ionization process. The cross-sections for non-resonant transitions are much lower than for transitions to autoionizing states meaning very high laser intensities are required to drive them efficiently. The limited tunability of the broadband Titanium:Sapphire laser in the wavelength region ($\leq$ 700 nm in fundamental wavelength) did not allow an easy search of autoionizing states in the vicinity of the ionization potential. However, the dye lasers utilize a grating for the wavelength selection thus making long-range wavelengths scans feasible within the gain band of the dye solution. Fig. 5 presents a scan of the second step laser (Dye 2 in Fig. 1) showing two prominent autoionizing states in the region between 282 and 288 nm. The additional features present in the figure arise from a single-color ionization channels starting from low-lying thermally excited states followed by transitions to intermediate states, listed in Table 1. In addition to the marked transitions, there are features below the leftmost autoionizing peak, that may be related to the intermediate states from which the ionization probability is low. The ion signal due to these ionization channels was also visible when the scan was performed without the first step laser. These transitions were furthermore used to re-calibrate the spectra as the scan was performed using the dye lasers low-accuracy internal wavelength calibration.

The measurement of the hyperfine spectra for the transition $4d^4 5s\ a\ {}^6D^0_{1/2} \rightarrow 4d^3 5s5p\ y\ {}^6D_{1/2}$ was performed by tuning the Master laser frequency and measuring the corresponding ion signal. The Toptica DL Pro Master laser operates in Littrow configuration; meaning frequency is tuned by tilting a grating with a Piezo actuator. In order to scan the laser a continuous sawtooth ramp, generated by a SC 110 HV scan generator in a Toptica SYS DC 110 control unit, was applied to the actuator. Furthermore, the mode-hop free scan range was extended by controlling the current with a feed-forward scheme.

During a scan, the wavelength was monitored either directly from the Master laser output or sampled from the output of Slave laser. Due to the continuous scanning mode, the ion counts were recorded every 100 ms to minimize lag induced artifacts in the spectra. Fig. 6 presents the hyperfine spectra for niobium for the 386.4016 nm transition measured with both narrowband (black dots) and broadband lasers (blue dots). The second step laser wavelength was set to 286.731 nm for the transition into the autoionizing state presented in Fig. 5.

The measured spectra were fitted with a calculated hyperfine spectrum using an analytical approximation to Voigt profile given in Ref. [40] as the lineshape. The F-state frequencies for the calculated spectra were given by

$$\Delta\nu = A \times \frac{C}{2} + B \times \frac{3C(C+1) - 4I(I+1)J(J+1)}{8I(2I-1)J(2J-1)}, \quad (1)$$

where J is the spin of the atomic state, I is the nuclear spin, A and B are the hyperfine coupling constants. Furthermore, $C = (F(F+1) - I(I+1) - J(J+1))$, where F is the spin of a hyperfine state. The fit yields a linewidth of 434.5 ± 7.4 MHz with a Gaussian and Lorentzian components of 394.0 ± 6.4 MHz and 73.0 ± 6.4 MHz, respectively. The Gaussian component is mainly due to the residual Doppler broadening in the reference cell. The laser linewidth contribution to the Doppler width is about 40 MHz due to the laser being operated in second harmonic. The remaining Lorentzian component is a result of power broadening.

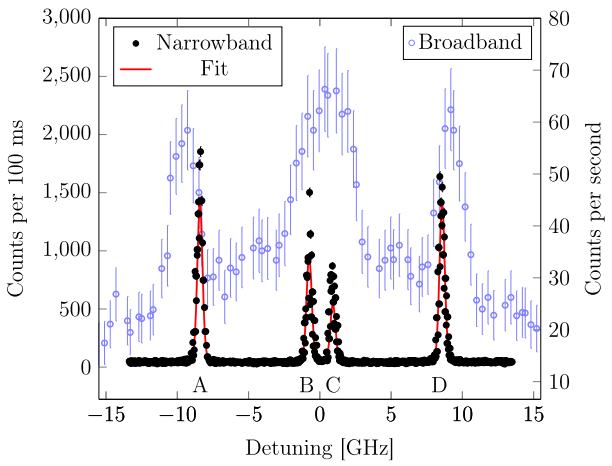

Fig. 6. Hyperfine spectra for ^{93}Nb measured both with the injection-locked laser and a broadband dye laser. The transitions labels correspond to the ones given in Fig. 4. (For interpretation of the references to color in this figure legend, the reader is referred to the web version of this article.)

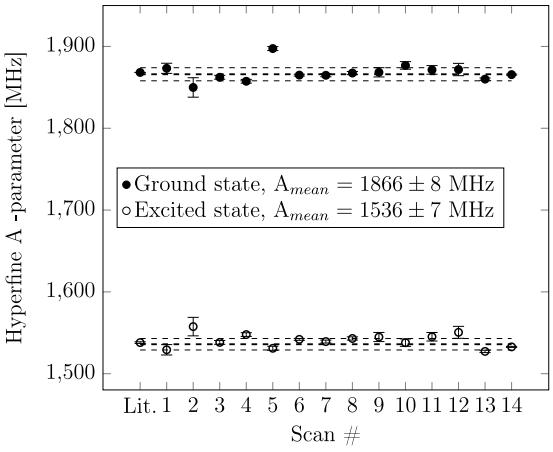

Fig. 7. The ground and excited state magnetic hyperfine coupling constants for multiple scans compared to the literature values. The dashed lines indicate the weighted mean value and the associated standard deviation of the mean.

Numerous scans were performed with various power settings, and laser combinations to maximize the signal and minimize possible laser power related broadening effects. This also enabled the extraction of a number of values for the magnetic hyperfine coupling constants for the ground and the excited state. Fig. 7 presents the coupling constants for multiple successive laser scans. The weighted mean of these values, 1866 ± 8 MHz for the ground state and 1536 ± 7 MHz for the excited state, agrees well with the literature values indicating the laser system is suited for producing high-resolution RIS-data in future experiments. Furthermore, a broadband laser scan performed with a dye laser is also presented in Fig. 6. A fit to the broadband spectra yielded a FWHM of ~5.7 GHz and magnetic coupling constants of 1920 ± 117 MHz and 1772 ± 114 MHz for the ground state and the excited state, respectively, highlighting a superior accuracy and resolution of the injection-locked laser.

5. In-jet RIS resolution estimation

The 1.5 to 5 GHz fundamental linewidth available from the standard laser at PALIS is optimal for efficient resonance ionization in-gas-cell,

Table 1
The low-lying thermally populated states [39] enabling the single-color ionization channels.

Id	Wavelength [nm]	Lower state energy [cm^{-1}]	Configuration	Upper state energy [cm^{-1}]]	Configuration
1	282.6011	2154.110	$5s^2\ a^4F_{7/2}$	37 539.670	$5p\ t^4F_{7/2}$
2	282.7301	2154.110	$5s^2\ a^4F_{7/2}$	37 523.530	$5p\ u^4G_{9/2}$
3	284.1765	2154.110	$5s^2\ a^4F_{7/2}$	37 343.500	$5p\ u^4G_{7/2}$
4	285.5005	2805.360	$5s^2\ a^4F_{9/2}$	37 831.580	$5p\ t^4F_{9/2}$
5	286.0801	2805.360	$5s^2\ a^4F_{7/2}$	37 760.600	$5p\ u^4G_{11/2}$

however, it may be limiting resolution in in-jet RIS compared to a narrowband laser. In order to estimate the in-jet RIS resolution in a counter-propagating geometry utilizing a third harmonic of a injection-locked laser, a rate-equations based ionization model was developed. The model simulates a 2-step ionization process with full hyperfine structure and non-resonant ionization step described by a set of differential equations [41] $\frac{dN_i}{dt}$, $\frac{dM_f}{dt}$, and $\frac{dIon_f}{dt}$ corresponding to the ground, excited, and ionized state, respectively. Here, the population in the Ion_f state is proportional to the ionization efficiency.

$$\begin{aligned}
\frac{dN_i}{dt} &= \sum_f \left(W_{i\rightleftarrows f} + A_{f\rightarrow i}\right) M_f - \sum_f W_{i\rightleftarrows f} N_i \\
\frac{dM_f}{dt} &= \sum_i W_{i\rightleftarrows f} N_i - \sum_i \left(W_{i\ \rightleftarrows f} + A_{f\rightarrow i}\right) M_f - R_{nr} M_f \\
\frac{dIon_f}{dt} &= \sum R_{nr} M_f,
\end{aligned} \tag{2}$$

where

$$\begin{aligned}
W_{f\rightleftarrows i}\left(\omega_L, F_i, F_f, t\right) = A_{f\rightarrow i} &\frac{\lambda_0^2}{4}\frac{E_0}{\omega_0 \hbar}\frac{(2F_f+1)(2F_i+1)}{2I+1} \\
&\times \begin{Bmatrix} J_f & F_f & I \\ F_i & J_i & 1 \end{Bmatrix} \\
&\times L_{\text{Voigt}}\left(\sigma_L, \sigma_G, \omega_L, \omega_0\right) \\
&\times G(t, \Gamma_L^n)
\end{aligned} \tag{3}$$

and

$$R_{nr} = \frac{E_{nr}}{\omega_{nr}\hbar}\sigma_{nr} \times G(t, \Gamma_L^{nr}). \tag{4}$$

Above, the transition rates for the allowed resonant transitions are denoted with $W_{i\rightleftarrows f}$, the spontaneous transition rate with A_f, and the non-resonant transition rate with R_f. ω_L is the laser frequency, λ_0 and ω_0 are the resonant wavelength and frequency, respectively. E_0 and E_{nr} correspond to the first step laser and the ionizing laser energy per pulse per cm^2. ω_{nr} is the frequency of the ionizing laser and σ_{nr} the cross-section for the transition.

$L_{\text{Voigt}}\left(\sigma_L, \sigma_G, \omega_L, \omega_0\right)$ is a Voigt spectral lineshape , described with Gaussian σ_G and Lorentzian σ_L widths. $G(t, \Gamma_L, \Delta_L)$ describes a Gaussian time profile of the laser pulse with a width of Γ_L. A rate-equation based model was chosen instead of a more advanced model, such as presented in Ref. [42], as the aim was to study the effect of the ionization environment to the resolution rather than detailed study of the RIS process.

The model (Eq. (2)) was written in Julia programming language [43], in which the set of differential equations were generated corresponding to the Cu ionization scheme (see Refs. [4] and [44]). Cu was chosen for the simulation as it is well studied experimentally, and has known pressure shift and broadening coefficients of 5.4 GHz and −1.9 GHz, respectively [6]. Here, the atomic and nuclear spins, and hyperfine coefficients for ^{63}Cu were utilized. The initial populations for the ground state F states was set to 0.5 and 0 for all the excited levels.

The model was applied to a copper atom tracks in a argon gas flow that were pre-simulated for geometry similar to PALIS presented in Ref. [22]. While he atom tracks begin from a high pressure (1000 mbar) gas cell region, followed by a 2 mm exit hole and a low-pressure region within a radiofrequency sextupole, the model was only applied to a points randomly selected from the track segments within the sextupole ion guide. The laser interaction region was a 2 mm wide cylinder with a Gaussian distribution along the sextupole axis. The laser pulse energies was kept low to avoid saturation effects.

Table 2
Model parameters.

I	3/2
J_i	1/2
J_f	1/2
A	5858 MHz
B	2432 MHz
$A_{f\rightarrow i}$	$2.030 \cdot 10^6$ 1/s
E_0	1 μJ/cm^2
E_{nr}	100 μ J/cm^2
ω_a	1227.462 THz
λ_a	244.164 nm
$\omega_n r$	679.8 THz
Γ_L^r	30 ns
$\Gamma_L^n r$	7 ns
σ_{nr}	$6.2 \cdot 10^{-14}$ cm^2
σ_L	1 MHz
σ_G	60 MHz

The atom velocity and direction, and the pressure and temperature of the gas flow was extracted for the selected points. These were used to apply the Doppler shift and pressure shift to the transition frequency ω_0, and wavelength λ_0, calculated with the help Eq. (1) and the center of gravity frequency and wavelength, ω_a and λ_a, respectively. Furthermore, both pressure and Doppler broadening effects were applied to the corresponding widths σ_G and σ_L when calculating the Voigt profile in Eq. (3).

The model was solved with Sundials [45] CVODES solver via DifferentialEquations.jl [46] wrapper package for about 70 track points, each with 500 frequency points ω_L evenly distributed around ω_a with a 30 GHz range. The parameters utilized in the model are presented in Table 2. An average of the population fraction at the state Ion_f yielded the final spectrum presented in Fig. 8. The FWHM of about 1400 MHz is for a considerable part due to the velocity distribution in-jet. This is only about a factor of 4 higher than the current state of the art for in-jet RIS [14], and demonstrates that narrowband laser discussed in this article will provide tangible benefits for the in-jet RIS at PALIS. The counter-propagating ionization geometry used in this estimation offers the most optimal gas-jet-laser overlap, however, a crossed-beam geometry would allow higher resolution due to narrower velocity distribution.

6. Conclusion and outlook

An injection-locked Titanium:Sapphire has been built in for high-resolution resonance ionization spectroscopy in-gas-jet at the PALIS system in RIKEN. Numerous advancements such as mounting the cavity mirrors directly on the baseplate and positioning the laser feet to minimize the vibration sensitivity have been implemented into the design to improve stability and usability.

The laser cavity was designed for flexibility. It can be reconfigured to two different lengths and crystal locations to operate the laser with different pulse width and gain modes. The longer cavity round-trip configuration includes a possibility to extend the tuning range using birefringent plates and intra-cavity second harmonic generation option. The latter option can lead to increased second harmonic and, more

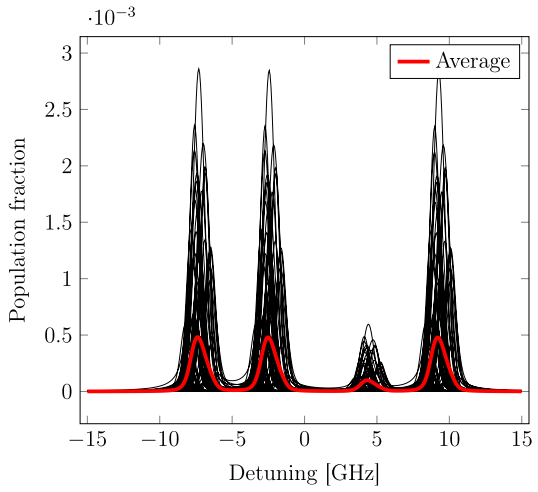

Fig. 8. Numerically estimated in-jet RIS resolution at PALIS. The red curve represents the average over all individual spectra (black). (For interpretation of the references to color in this figure legend, the reader is referred to the web version of this article.)

importantly, it produces high-quality beams required by the long laser transport path at PALIS.

The laser has been demonstrated to perform as designed with a tuning range across the whole Master laser range. Importantly, the laser was successfully applied to hyperfine spectroscopy of ^{93}Nb. These measurements yielded a total FWHM of 434.5 ± 7.4 MHz and a magnetic hyperfine coupling constants of 1866 ± 8 MHz for the ground state and 1536 ± 7 MHz for the first excited state in a good agreement with the literature values [27]. Additionally, the work led to a discovery of two prominent autoionizing transitions from the first excited state. Possible future goals for niobium include the determination of the efficiency of the newly developed ionization scheme and apply it for RIS of radioactive niobium isotopes. Moreover, the possibility to separate the ^{93m}Nb isomer from the ground state for the application in integrated fast neutron dosimetry [28,34] is to be studied. In conclusions, the injection-locked Titanium:Sapphire laser system has been demonstrated to be ready for high-resolution in-gas-jet spectroscopy at the PALIS in the near future both through experimental and numerical methods.

Acknowledgments

This work was supported by Japan Society for the Promotion of Science (JSPS) Postdoctoral Fellowship for Foreign Researchers, Japan program P14735 and Academy of Finland Postdoctoral Researcher, Finland project 296323.

References

[1] E.W. Otten, Nuclear radii and moments of unstable isotopes, in: D.A. Bromley (Ed.), Treatise on Heavy Ion Science: Volume 8: Nuclei Far From Stability, Springer US, Boston, MA, 1989, pp. 517–638.

[2] P. Campbell, I. Moore, M. Pearson, Laser spectroscopy for nuclear structure physics, Prog. Part. Nucl. Phys. 86 (2016) 127–180, http://dx.doi.org/10.1016/j.ppnp.2015.09.003, URL http://www.sciencedirect.com/science/article/pii/S0146641015000915.

[3] V. Lethokov, Laser Photoionization Spectroscopy, Academic Press, Orlando, 1987.

[4] T.E. Cocolios, A.N. Andreyev, B. Bastin, N. Bree, J. Büscher, J. Elseviers, J. Gentens, M. Huyse, Y. Kudryavtsev, D. Pauwels, T. Sonoda, P. Van den Bergh, P. Van Duppen, Magnetic dipole moment of ^{57,59}Cu measured by in-gas-cell laser spectroscopy, Phys. Rev. Lett. 103 (2009) 102501, http://dx.doi.org/10.1103/PhysRevLett.103.102501, URL http://link.aps.org/doi/10.1103/PhysRevLett.103.102501.

[5] M. Laatiaoui, W. Lauth, H. Backe, M. Block, D. Ackermann, B. Cheal, P. Chhetri, C.E. Düllmann, P. van Duppen, J. Even, R. Ferrer, F. Giacoppo, S. Götz, F.P. Heßberger, M. Huyse, O. Kaleja, J. Khuyagbaatar, P. Kunz, F. Lautenschläger, A.K. Mistry, S. Raeder, E.M. Ramirez, T. Walther, C. Wraith, A. Yakushev, Atom-at-a-time laser resonance ionization spectroscopy of nobelium, Nature 538 (7626) (2016) 495–498, http://dx.doi.org/10.1038/nature19345.

[6] T. Sonoda, T. Cocolios, J. Gentens, M. Huyse, O. Ivanov, Y. Kudryavtsev, D. Pauwels, P.V. den Bergh, P.V. Duppen, The Laser Ion Source Trap (LIST) coupled to a gas cell catcher, Nucl. Instrum. Methods Phys. Res. B 267 (17) (2009) 2918–2926, http://dx.doi.org/10.1016/j.nimb.2009.06.085, URL http://www.sciencedirect.com/science/article/pii/S0168583X09007812.

[7] M. Reponen, I. Moore, I. Pohjalainen, T. Kessler, P. Karvonen, J. Kurpeta, B. Marsh, S. Piszczek, V. Sonnenschein, J. Äystö, Gas jet studies towards an optimization of the IGISOL LIST method, Nucl. Instrum. Methods Phys. Res. A 635 (1) (2011) 24–34, http://dx.doi.org/10.1016/j.nima.2011.01.125, URL http://www.sciencedirect.com/science/article/pii/S0168900211002117.

[8] Y. Kudryavtsev, R. Ferrer, M. Huyse, P.V. den Bergh, P.V. Duppen, The in-gas-jet laser ion source: Resonance ionization spectroscopy of radioactive atoms in supersonic gas jets, Nucl. Instrum. Methods Phys. Res. B 297 (Supplement C) (2013) 7–22, http://dx.doi.org/10.1016/j.nimb.2012.12.008, URL http://www.sciencedirect.com/science/article/pii/S0168583X12007525.

[9] V. Sonnenschein, Laser Developments and High Resolution Resonance Ionization Spectroscopy of Actinide Elements (Ph.D. thesis), The University of Jyväskylä, 2015.

[10] V. Sonnenschein, I.D. Moore, S. Raeder, M. Reponen, H. Tomita, K. Wendt, Characterization of a pulsed injection-locked Ti:sapphire laser and its application to high resolution resonance ionization spectroscopy of copper, Laser Phys. 27 (8) (2017) 085701, URL http://stacks.iop.org/1555-6611/27/i=8/a=085701.

[11] V. Sonnenschein, I.D. Moore, S. Raeder, A. Hakimi, A. Popov, K. Wendt, The search for the existence of ^{229m}Th at IGISOL, Eur. Phys. J. A 48 (4) (2012) 52, http://dx.doi.org/10.1140/epja/i2012-12052-3.

[12] S. Raeder, B. Bastin, M. Block, P. Creemers, P. Delahaye, R. Ferrer, X. Fléchard, S. Franchoo, L. Ghys, L. Gaffney, C. Granados, R. Heinke, L. Hijazi, M. Huyse, T. Kron, Y. Kudryavtsev, M. Laatiaoui, N. Lecesne, F. Luton, I. Moore, Y. Martinez, E. Mogilevskiy, P. Naubereit, J. Piot, S. Rothe, H. Savajols, S. Sels, V. Sonnenschein, E. Traykov, C.V. Beveren, P.V. den Bergh, P.V. Duppen, K. Wendt, A. Zadvornaya, Developments towards in-gas-jet laser spectroscopy studies of actinium isotopes at LISOL, Nucl. Instrum. Methods Phys. Res. B 376 (2016) 382–387, http://dx.doi.org/10.1016/j.nimb.2015.12.014, Proceedings of the XVIIth International Conference on Electromagnetic Isotope Separators and Related Topics (EMIS2015), Grand Rapids, MI, U.S.A., 11-15 May 2015. URL http://www.sciencedirect.com/science/article/pii/S0168583X15012586.

[13] A. Voss, V. Sonnenschein, P. Campbell, B. Cheal, T. Kron, I.D. Moore, I. Pohjalainen, S. Raeder, N. Trautmann, K. Wendt, High-resolution laser spectroscopy of long-lived plutonium isotopes, Phys. Rev. A 95 (2017) 032506, http://dx.doi.org/10.1103/PhysRevA.95.032506, URL https://link.aps.org/doi/10.1103/PhysRevA.95.032506.

[14] R. Ferrer, A. Barzakh, B. Bastin, R. Beerwerth, M. Block, P. Creemers, H. Grawe, R. de Groote, P. Delahaye, X. Fléchard, S. Franchoo, S. Fritzsche, L.P. Gaffney, L. Ghys, W. Gins, C. Granados, R. Heinke, L. Hijazi, M. Huyse, T. Kron, Y. Kudryavtsev, M. Laatiaoui, N. Lecesne, M. Loiselet, F. Lutton, I.D. Moore, Y. Martínez, E. Mogilevskiy, P. Naubereit, J. Piot, S. Raeder, S. Rothe, H. Savajols, S. Sels, V. Sonnenschein, J.C. Thomas, E. Traykov, C. Van Beveren, P. Van den Bergh, P. Van Duppen, K. Wendt, A. Zadvornaya, Towards high-resolution laser ionization spectroscopy of the heaviest elements in supersonic gas jet expansion, Nature Commun. 8 (2017) 14520+, http://dx.doi.org/10.1038/ncomms14520.

[15] K.T. Flanagan, K.M. Lynch, J. Billowes, M.L. Bissell, I. Budinčević, T.E. Cocolios, R.P. de Groote, S. De Schepper, V.N. Fedosseev, S. Franchoo, R.F. Garcia Ruiz, H. Heylen, B.A. Marsh, G. Neyens, T.J. Procter, R.E. Rossel, S. Rothe, I. Strashnov, H.H. Stroke, K.D.A. Wendt, Collinear resonance ionization spectroscopy of neutron-deficient francium isotopes, Phys. Rev. Lett. 111 (2013) 212501, http://dx.doi.org/10.1103/PhysRevLett.111.212501, URL https://link.aps.org/doi/10.1103/PhysRevLett.111.212501.

[16] R.P. de Groote, J. Billowes, C.L. Binnersley, M.L. Bissell, T.E. Cocolios, T. Day Goodacre, G.J. Farooq-Smith, D.V. Fedorov, K.T. Flanagan, S. Franchoo, R.F. Garcia Ruiz, A. Koszorús, K.M. Lynch, G. Neyens, F. Nowacki, T. Otsuka, S. Rothe, H.H. Stroke, Y. Tsunoda, A.R. Vernon, K.D.A. Wendt, S.G. Wilkins, Z.Y. Xu, X.F. Yang, Dipole and quadrupole moments of $^{73-78}$Cu as a test of the robustness of the $Z = 28$ shell closure near ^{78}Ni, Phys. Rev. C 96 (2017) 041302, http://dx.doi.org/10.1103/PhysRevC.96.041302, URL https://link.aps.org/doi/10.1103/PhysRevC.96.041302.

[17] M. Wada, A. Takamine, K. Okada, T. Sonoda, P. Schury, V. Lioubimov, Y. Yamazaki, Y. Kanai, T.M. Kojima, A. Yoshida, T. Kubo, H. Iimura, I. Katayama, S. Ohtani, H. Wollnik, H.A. Schuessler, Universal Slow RI-Beam Facility at RIKEN RIBF for Laser spectroscopy of short-lived nuclei, AIP Conf. Proc. 1104 (1) (2009) 16–21, http://dx.doi.org/10.1063/1.3115596, arXiv:http://aip.scitation.org/doi/pdf/10.1063/1.3115596. URL http://aip.scitation.org/doi/abs/10.1063/1.3115596.

[18] T. Kubo, In-flight RI beam separator BigRIPS at RIKEN and elsewhere in Japan, Nucl. Instrum. Methods Phys. Res. B 204 (2003) 97–113, http://dx.doi.org/10.1016/S0168-583X(02)01896-7, 14th International Conference on Electromagnetic Isotope Separators and Techniques Related to their Applications. URL http://www.sciencedirect.com/science/article/pii/S0168583X02018967.

[19] P. Schury, M. Wada, Y. Ito, F. Arai, S. Naimi, T. Sonoda, H. Wollnik, V. Shchepunov, C. Smorra, C. Yuan, A high-resolution multi-reflection time-of-flight mass spectrograph for precision mass measurements at RIKEN/SLOWRI, Nucl. Instrum. Methods Phys. Res. B 335 (2014) 39–53, http://dx.doi.org/10.1016/j.nimb.2014.05.016, URL http://www.sciencedirect.com/science/article/pii/S0168583X1400559X.

[20] A. Takamine, M. Wada, K. Okada, T. Sonoda, P. Schury, T. Nakamura, Y. Kanai, T. Kubo, I. Katayama, S. Ohtani, H. Wollnik, H.A. Schuessler, Hyperfine structure constant of the neutron halo nucleus $^{11}Be^{+}$, Phys. Rev. Lett. 112 (2014) 162502, http://dx.doi.org/10.1103/PhysRevLett.112.162502, URL https://link.aps.org/doi/10.1103/PhysRevLett.112.162502.

[21] T. Sonoda, M. Wada, A. Takamine, K. Okada, P. Schury, A. Yoshida, T. Kubo, Y. Matsuo, T. Furukawa, T. Wakui, T. Shinozuka, H. Iimura, Y. Yamazaki, I. Katayama, S. Ohtani, H. Wollnik, H.A. Schuessler, Y. Kudryavtsev, P.V. Duppen, M. Huyse, S. Collaboration, Restoration of RI-beams from a projectile fragment separator by Laser Ionization gas Catcher -PALIS-, AIP Conf. Proc. 1104 (1) (2009) 132–137, http://dx.doi.org/10.1063/1.3115589, arXiv:http://aip.scitation.org/doi/pdf/10.1063/1.3115589. URL http://aip.scitation.org/doi/abs/10.1063/1.3115589.

[22] T. Sonoda, M. Wada, H. Tomita, C. Sakamoto, T. Takatsuka, T. Furukawa, H. Iimura, Y. Ito, T. Kubo, Y. Matsuo, H. Mita, S. Naimi, S. Nakamura, T. Noto, P. Schury, T. Shinozuka, T. Wakui, H. Miyatake, S. Jeong, H. Ishiyama, Y. Watanabe, Y. Hirayama, K. Okada, A. Takamine, Development of a resonant laser ionization gas cell for high-energy, short-lived nuclei, Nucl. Instrum. Methods Phys. Res. B 295 (Supplement C) (2013) 1–10, http://dx.doi.org/10.1016/j.nimb.2012.10.009, URL http://www.sciencedirect.com/science/article/pii/S0168583X12006465.

[23] T. Sonoda, H. Iimura, M. Reponen, M. Wada, I. Katayama, V. Sonnenschein, T. Takamatsu, H. Tomita, T. Kojima, The laser and optical system for the RIBF-PALIS experiment, Nucl. Instrum. Methods Phys. Res. A 877 (Supplement C) (2018) 118–123, http://dx.doi.org/10.1016/j.nima.2017.09.055, URL http://www.sciencedirect.com/science/article/pii/S0168900217310252.

[24] T. Sonoda, T. Tsubota, M. Wada, I. Katayama, T.M. Kojima, M. Reponen, A gas circulation and purification system for gas-cell-based low-energy RI-beam production, Rev. Sci. Instrum. 87 (6) (2016) 065104, http://dx.doi.org/10.1063/1.4953111, arXiv:https://doi.org/10.1063/1.4953111.

[25] T. Kessler, H. Tomita, C. Mattolat, S. Raeder, K. Wendt, An injection-seeded high-repetition rate Ti:Sapphire laser for high-resolution spectroscopy and trace analysis of rare isotopes, Laser Phys. 18 (7) (2008) 842, http://dx.doi.org/10.1134/S1054660X08070074.

[26] H. Tomita, C. Mattolat, T. Kessler, S. Raeder, F. Schwellnus, K.D.A. Wendt, K. Watanabe, T. Iguichi, Ultra Trace determination scheme for 26 Al by high-resolution resonance ionization mass spectrometry using a pulsed Ti:Sapphire laser, J. Nucl. Sci. Technol. 45 (sup6) (2008) 37–42, http://dx.doi.org/10.1080/00223131.2008.10875974, arXiv:https://doi.org/10.1080/00223131.2008.10875974.

[27] A. Bouzed, S. Kröger, D. Zimmermann, H.D. Kronfeldt, G. Guthöhrlein, Hyperfine structure in the atomic spectrum of niobium, Eur. Phys. J. D 23 (1) (2003) 57–62, http://dx.doi.org/10.1140/epjd/e2003-00026-8.

[28] H.M. Lauranto, I.H. Auterinen, T.T. Kajava, K.M. Nyholm, R.R.E. Salomaa, Determination of hyperfine structures and Rydberg convergence limits of selected optical transitions in ^{93}Nb using resonance ionization spectroscopy, Appl. Phys. B 50 (4) (1990) 323–329, http://dx.doi.org/10.1007/BF00325067.

[29] D.M. Rayner, S.A. Mitchell, O.L. Bourne, P.A. Hackett, First-ionization potential of niobium and molybdenum by double-resonance, field-ionization spectroscopy, J. Opt. Soc. Amer. B 4 (6) (1987) 900–905, http://dx.doi.org/10.1364/JOSAB.4.000900, URL http://josab.osa.org/abstract.cfm?URI=josab-4-6-900.

[30] S. Kröger, I.K. Öztürk, F.G. Acar, G.C. Başar, G. Başar, J.F. Wyart, Fine and hyperfine structure in the atomic spectrum of niobium, Eur. Phys. J. D 41 (1) (2007) 61–70, http://dx.doi.org/10.1140/epjd/e2006-00207-y.

[31] B. Cheal, K. Baczynska, J. Billowes, P. Campbell, F.C. Charlwood, T. Eronen, D.H. Forest, A. Jokinen, T. Kessler, I.D. Moore, M. Reponen, S. Rothe, M. Rüffer, A. Saastamoinen, G. Tungate, J. Äystö, Laser spectroscopy of niobium fission fragments: First use of optical pumping in an ion beam cooler buncher, Phys. Rev. Lett. 102 (2009) 222501, http://dx.doi.org/10.1103/PhysRevLett.102.222501, URL https://link.aps.org/doi/10.1103/PhysRevLett.102.222501.

[32] H. Lauranto, Numerical studies of the isomer selectivity of two- and three-step resonance ionization of niobium, Appl. Phys. B 66 (2) (1998) 231–239, http://dx.doi.org/10.1007/s003400050381.

[33] T. Takatsuka, H. Tomita, T. Sonoda, V. Sonnenschein, C. Sakamoto, H. Mita, T. Noto, C. Ito, S. Maeda, T. Iguchi, M. Wada, K. Wendt, I. Moore, Deevelopment of high resolution resonance ionization mass spectrometry for trace analysis of ^{93m}Nb, Hyperfine Interact. 216 (1) (2013) 41–46, http://dx.doi.org/10.1007/s10751-013-0824-7.

[34] H. Tomita, T. Takatsuka, T. Takamatsu, Y. Adachi, Y. Furuta, T. Noto, T. Iguchi, V. Sonnenschein, K. Wendt, C. Ito, S. Maeda, Development of high resolution resonance ionization mass spectrometry for neutron dosimetry technique with ^{93}Nb(n,n')^{93m}Nb Reaction, EPJ Web Conf. 106 (2016) 05002, http://dx.doi.org/10.1051/epjconf/201610605002.

[35] H. Kogelnik, T. Li, Laser beams and resonators, Appl. Opt. 5 (10) (1966) 1550–1567, http://dx.doi.org/10.1364/AO.5.001550, URL http://ao.osa.org/abstract.cfm?URI=ao-5-10-1550.

[36] V. Sonnenschein, I.D. Moore, I. Pohjalainen, M. Reponen, S. Rothe, K. Wendt, Intracavity frequency doubling and difference frequency mixing for pulsed ns Ti:Sapphire laser systems at on-line radioactive ion beam facilities, in: Proceedings of the Conference on Advances in Radioactive Isotope Science (ARIS2014), arXiv:http://journals.jps.jp/doi/pdf/10.7566/JPSCP.6.030126 http://doi.org/10.7566/JPSCP.6.030126, URL http://journals.jps.jp/doi/abs/10.7566/JPSCP.6.030126.

[37] J. Sauvage, N. Boos, L. Cabaret, J. Crawford, H. Duong, J. Genevey, M. Girod, G. Huber, F. Ibrahim, M. Krieg, F. Le Blanc, J. Lee, J. Libert, D. Lunney, J. Obert, J. Oms, S. Péru, J. Pinard, J. Putaux, B. Roussière, V. Sebastian, D. Verney, S. Zemlyanoi, J. Arianer, N. Barré, M. Ducourtieux, D. Forkel-Wirth, G. Le Scornet, J. Lettry, C. Richard-Serre, C. Véron, Complis experiments: collaboration for spectroscopy measurements using a pulsed laser ion source, Hyperfine Interact. 129 (1) (2000) 303–317, http://dx.doi.org/10.1023/A:1012618001695.

[38] H. Lauranto, T. Kajava, R. Salomaa, Hyperfine structure studies of ^{93}nb by three-step resonance ionization spectroscopy, Spectrochim. Acta, Part B 51 (1) (1996) 175–180, http://dx.doi.org/10.1016/0584-8547(95)01392-X, URL http://www.sciencedirect.com/science/article/pii/058485479501392X.

[39] R. Kurucz, B. Bell, Atomic Line Data, in: Atomic Line Data (R.L. Kurucz and B. Bell) Kurucz CD-ROM No. 23, Vol. 23, Smithsonian Astrophysical Observatory, Cambridge, Mass, 1995.

[40] A. McLean, C. Mitchell, D. Swanston, Implementation of an efficient analytical approximation to the voigt function for photoemission lineshape analysis, J. Electron Spectrosc. Relat. Phenom. 69 (2) (1994) 125–132, http://dx.doi.org/10.1016/0368-2048(94)02189-7, URL http://www.sciencedirect.com/science/article/pii/0368204894021897.

[41] H. Backe, A. Dretzke, S. Fritzsche, R.G. Haire, P. Kunz, W. Lauth, M. Sewtz, N. Trautmann, Laser spectroscopic investigation of the element fermium (z = 100), Hyperfine Interact. 162 (1) (2005) 3–14, http://dx.doi.org/10.1007/s10751-005-9209-x.

[42] R.P. de Groote, M. Verlinde, V. Sonnenschein, K.T. Flanagan, I. Moore, G. Neyens, Efficient, high-resolution resonance laser ionization spectroscopy using weak transitions to long-lived excited states, Phys. Rev. A 95 (2017) 032502, http://dx.doi.org/10.1103/PhysRevA.95.032502, URL https://link.aps.org/doi/10.1103/PhysRevA.95.032502.

[43] J. Bezanson, A. Edelman, S. Karpinski, V. Shah, Julia: a fresh approach to numerical computing, SIAM Rev. 59 (1) (2017) 65–98, http://dx.doi.org/10.1137/141000671, arXiv:https://doi.org/10.1137/141000671.

[44] Y. Kudryavtsev, R. Ferrer, M. Huyse, P. Van den Bergh, P. Van Duppen, L. Vermeeren, Two-step laser ionization schemes for in-gas laser ionization and spectroscopy of radioactive isotopes, Rev. Sci. Instrum. 85 (2) (2014) 02B915, http://dx.doi.org/10.1063/1.4850695, arXiv:https://doi.org/10.1063/1.4850695.

[45] A.C. Hindmarsh, P.N. Brown, K.E. Grant, S.L. Lee, R. Serban, D.E. Shumaker, C.S. Woodward, SUNDIALS: Suite of nonlinear and differential/algebraic equation solvers, ACM Trans. Math. Softw. (TOMS) 31 (3) (2005) 363–396.

[46] C. Rackauckas, Q. Nie, Differentialequations.jl a performant and feature-rich ecosystem for solving differential equations in julia, J. Open Res. Softw. 5(1) (2017) 15, http://dx.doi.org/10.5334/jors.151.